LRP 267/85

Papers contributed to the

12th EUROPEAN CONFERENCE ON CONTROLLED

FUSION AND PLASMA PHYSICS

Budapest, Hungary, September 1985

STRONG ELECTRON AND ION HEATING IN CLEAN CONDITIONS IN TCA

A. de Chambrier, G.A. Collins, B. Joye, A. Lietti, J.B. Lister and J.-M. Moret
Centre de Recherches en Physique des Plasmas
Association Euratom - Confédération Suisse
Ecole Polytechnique Fédérale de Lausanne
21, Av. des Bains, CH-1007 Lausanne, Switzerland

Abstract. Recent results from the Alfvén Wave Heating experiments (2.5 MHz) on the TCA Tokamak show extremely strong sawtooth activity above the AW continuum thresholds. The power deposition profile to the electrons appears to be very peaked in these conditions. Below dominant AW thresholds, we have measured anomalously strong increases in ion temperature, reaching 17 x 10^{13} eV/kWcm^3.

I. Electron Heating. AWH experiments are currently underway on the TCA tokamak (R,a = 0.61,0.18 m, B_ϕ = 1.5T, I_p ~ 130 kA). Using new SiC limiters and lateral screens we had obtained very clean conditions with sustained electron heating and a drop in loop voltage during the rf pulse[1]. The cost of installing side screens was a reduction of the antenna loading and hence of the available rf power. We therefore removed these screens to carry out the work described at 200-230 kW, greater than the ohmic power in the target plasma. Even with the measured increase in radiated power loss during the rf pulse, the loss on axis does not increase until 13 msec into the rf pulse[2], representing a few electron energy confinement times at low density. The electron energy balance could therefore be studied convincingly during this period. The increase in T_e previously obtained[1] showed a large dispersion which we subsequently found to be correlated with the sawtooth period. The electron temperature as a function of time in the period has been measured and repeated in three conditions, namely the OH target plasma, with the rf applied in the (n,m) = (2,0) continuum[3] and with the rf applied in the (n,m) = (2,1) continuum. Figure 1 shows the representative results obtained using a 1 pulse - 1 position Ruby scattering system. The central temperature was measured 7 msec after the start of the rf pulse, about 1-2 x τ_{Ee} under these conditions, so the electron energy balance was probably quasi-stationary. The electron temperature ramp (solid line) is the result of a linear fit to the data. These discharges were, in two cases, obtained only three days after the vessel was opened up to air, demonstrating the resiliance of the effect; no gettering is used in TCA. In Table I, we have in addition calculated 3/2 e x n_{eo} x $\tilde{\Delta T}_{eo}/\tilde{\Delta t}$ where $\tilde{\Delta T}_{eo}$ is the amplitude of the sawtooth of period $\tilde{\Delta t}$, with the central density measured using a multi-chord interferometer. The rf power quoted is the total power delivered from the antenna,

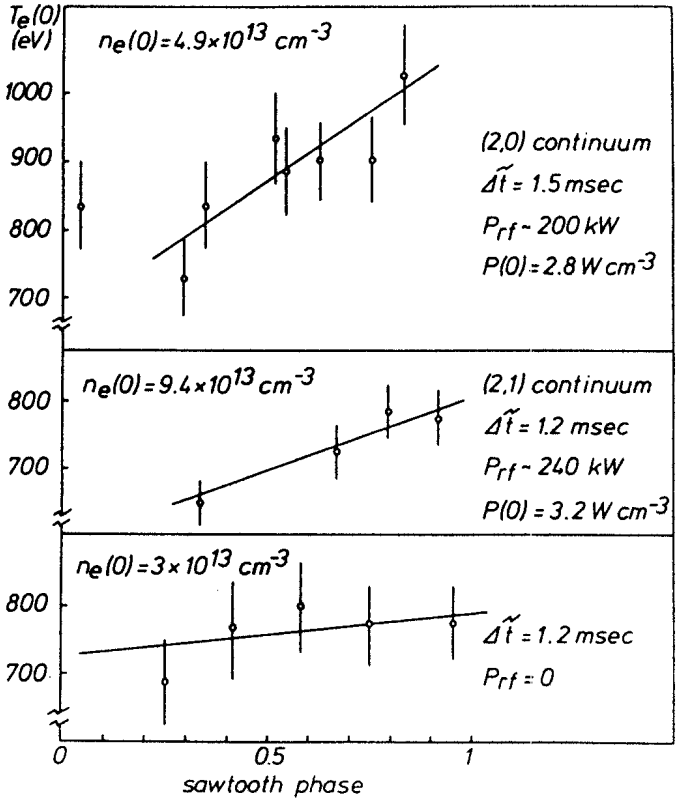

Fig. 1: Electron temperature increase measured during a sawtooth period, for different conditions.

uncorrected for coupling efficiency. The greatest increase is in the (2,0) continuum, with the (2,1) continuum almost as good. We have not included the term 3/2 e x T_{eo} x dn_{eo}/dt in the calculation of the electron energy increase, although the magnitude of the term is similar. The value of $\dot{W}_{eo}$ is conventionally[4-6] related to the central power deposition $P_{rf}(0)$, and we have compared our values of $P_{rf}(0)/\langle P_{rf}\rangle$ with these available references in Table II. The power deposition is clearly inferior to that obtained with ECRH[4] on PDX whose authors quote the major part of the incident power as being deposited within the q = 1 surface. The central deposition analysed according to these accepted, but not necessarily correct, assumptions is higher for AWH than for ICRH and NBI.

TABLE I

Case	n_{eo}(pre-rf) (x 10^{13} cm^{-3})	$\tilde{\Delta t}$ (msec)	$\tilde{\Delta T}_{eo}$ (eV)	P_{rf} (kW)	$P_{rf}(0)/\langle P_{rf}\rangle$
a - OH	3.0	1.2	60	-	-
b - (2,0)	4.7	1.2	420	195	8.0
c - (2,0)	4.9	1.5	360	200	5.5
d - (2,0)	5.2	1.5	300	195	5.0
e - (2,1)	9.4	1.2	202	265	5.6

TABLE II

Case	$\dot{W}(0)$ ($W\ cm^{-3}$)	P_{rf}(kW)	$P_{rf}(0)/\langle P_{rf}\rangle$
ECRH-PDX[4]	0.65	75	37
AWH-TCA	2.5-3.8	200-265	5.0-8.0
ICRH-PLT[6]	2.00	4300	1.94
ICRH-TEXTOR[5]	0.2	1000	1.46
NBI-DIII[7]	0.75	2100	2.16

In addition to these measurements we have also integrated the electron power balance equation in the presence of rf assuming both $n_e(r)\chi_e(r)$ and the temperature profiles to be unchanged from their ohmic values. This analysis showed that the missing power was greater than the delivered rf power, which translates to the deposition profile being more peaked than the divergence of the conducted energy flow. This is roughly the ohmic power deposition profile which has a value $P_{OH}(0)/\langle P_{OH}\rangle \sim q_a \sim 3.2$. The two approaches therefore support each other. The reasons for the strong core heating are not yet elucidated but it seems clear that the power deposition is not local to the (2,0) resonance layer, estimated to be at $r_s/a \sim 0.5$. The results suggest that the kinetic Alfvén wave which propagates inwards from the appropriate resonance surface, is able to deposit appreciable energy within the $q = 1$ surface at $r/a \sim 0.2$. The local kinetic Alfvén wavelength is roughly 2.5 cm for the lower density case.

II. Ion Heating. The first heating results[8] on TCA showed considerable ion heating, but not under the same conditions as the strongest electron heating quoted. This has now been very clearly shown by varying the conditions of plasma density, filling gas and applied AW "mode". A typical result is shown in Fig. 2 in which the ion temperature rate of increase stops at the AW threshold (n,m) = (2,0). This behaviour repeats itself below several AW thresholds. Fig. 2 shows the calculated value of $P_{ei}(0)$, assuming $Z_{eff} \sim 2.0$, and assuming $T_i \sim T_z$; the value of $\dot{W}_i(0)/P_{ei}(0)$ exceeds unity and this is a much more direct proof of ion heating than was available before[9]. The value of $\bar{n}\Delta T_i/P_{rf}$ is not particularly useful since the temperature increase is discontinuous and the density increases strongly, nonetheless the value measured reaches 17×10^{13} eV/kW cm^3. The results obtained at higher density are particularly relevant since the Neutral Particle Analyser is more reliable than at the low densities at which the signal is weaker. Two interpretations are open to us. Firstly, there can be direct ion heating from an rf wave and secondly there could still be an anomalous electron-ion equilibration rate. Until we reach $T_i > T_e$ we cannot exclude the latter, but it is clear that the anomaly factor would have to be of the order of 2-3 for the rf power used, and it would have to be sensitive to the Alfvén Wave Spectrum excited. The

mechanism which could lead to direct ion heating is unclear, although ion heating has already been observed in particle simulations of AWH[10]. Since the ion temperature increase stops abruptly above a AW resonance threshold, the heating may well be unrelated to the excitation of Shear Alfvén Waves.

Acknowledgements: We thank the whole TCA team for their assistance in this work, and are grateful to Professor F. Troyon and A. Heym for their support. The work was partly funded by the Fonds National Suisse.

References

[1] A. de Chambrier et al., F-III-3, X Int. Conf. IAEA, London (1984)
[2] B. Joye et al., paper presented at this conference
[3] K. Appert et al., Phys, Rev. Lett. 54 (1985) 1671.
[4] A. Cavallo et al., Nucl. Fusion 25, (1985) 335.
[5] R.R. Weynants et al., 6th Topical Conf. on Radio Frequency Plasma Heating, Georgia, USA (1985).
[6] A. Cavallo et al., ibid.
[7] F.B. Marcus et al., GA Technologies Report GA-A16960 (1983)
[8] A. de Chambrier et al., Plasma Physics 25 (1983) 1021.
[9] A. de Chambrier et al., Plasma Physics 26 (1984) 173.
[10] J.L. Geary et al., Bull. Am. Phys. Soc., 29, (1984) 1401.

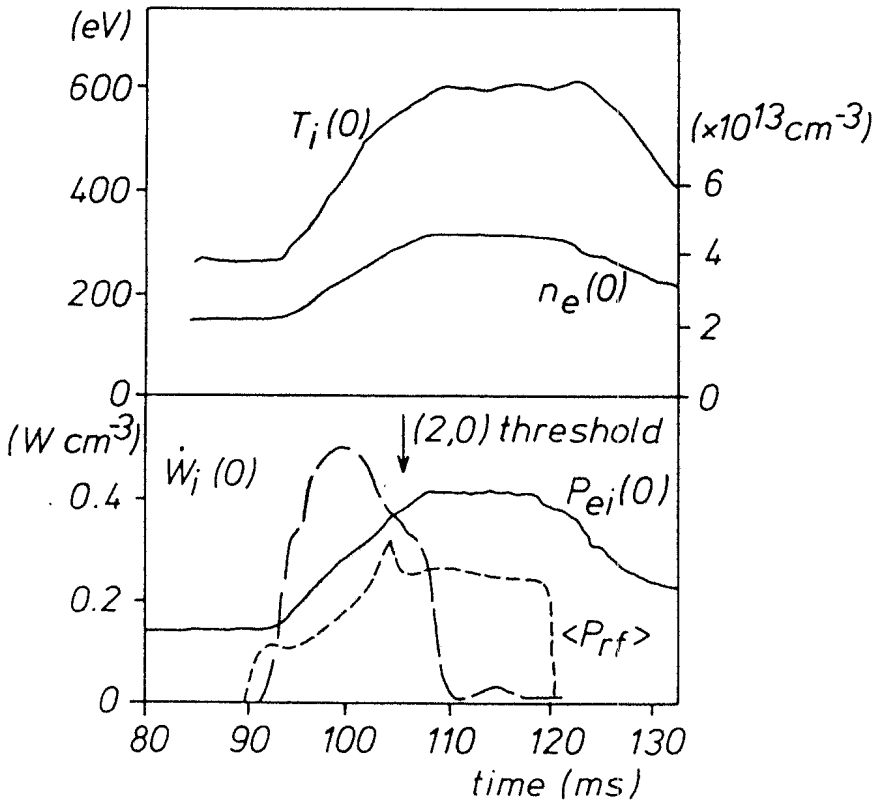

Fig. 2: Time evolution of the ion temperature, electron density, and central ion energy balance during the rf pulse.

A STUDY OF THE DENSITY RISE OBSERVED DURING AWH IN TCA

G.A. Collins, B. Joye, J.B. Lister and J.-M. Moret
Centre de Recherches en Physique des Plasmas
Association Euratom - Confédération Suisse
Ecole Polytechnique Fédérale de Lausanne
21, Av. des Bains, CH-1007 Lausanne, Switzerland

I. INTRODUCTION. One of the most striking consequences of Alfvén Wave Heating in TCA is a large increase in the electron density during the rf pulse. Although a small increase is characteristic of rf heating in ICRF[1] and lower hybrid current drive[2], the magnitude of the density increase seen during AWH is astonishing (up to 300% of the target density with 200 kW of rf power). Despite many changes to the design and materials of both the limiter and antenna, all of which have greatly modified the impurity behaviour and consequently the heating efficiency, the density rise has persisted since the earliest TCA experiments. In this paper, we document the density rise as a function of controllable parameters - target density, plasma current, rf power and antenna phasing - as well as discussing how such an increase could be explained by conventional models of particle balance.

II. DENSITY AND PROFILE BEHAVIOUR. The behaviour of the electron density under the influence of 100 kW of rf is shown in Fig. 1 which represents the standard TCA conditions: R,a = 0.61,0.18 m, B_ϕ = 1.5 T, I_p = 130 kA, graphite limiters and a hydrogen plasma. The antenna structure is usually

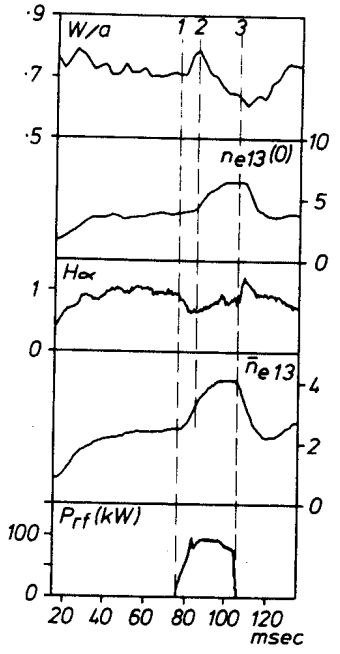

Fig.1 Typical hydrogen discharge with 100kW of rf

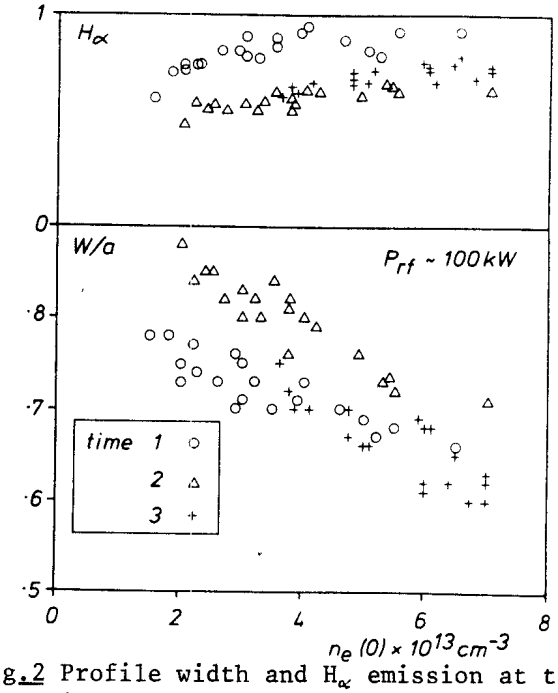

Fig.2 Profile width and H_α emission at times shown in Fig.1 for different target densities

phased to excite waves with dominant toroidal wavenumbers n = ±2 and poloidal wavenumbers m = ±1, at a frequency of 2.5 MHz. The target density is set up using feedback control of the gas valve and the rf power is applied when a stationary state has been reached. During the rf pulse the gas valve voltage is clamped at its pre-rf value, although little difference is observed in the qualitative effects of the high rf power on the density if the gas feed is cut to zero.

The evolution of the electron density profile is indicated in Fig. 1 by both the central electron density $n_e(0)$ and W, the profile half width at half maximum. Even though $n_e(0)$ begins rising immediately, the profile flattens during the first 7 ms, but then peaks to have a form typical of ohmic conditions. This is also shown in Fig. 2 for discharges at different target densities. Associated with the onset of the rf is a significant drop in the line-integrated H_α emission which then increases slowly, reflecting the overall rise in electron density but never reaching the equivalent ohmic level (Fig. 2). A qualitatively similar H_α signal is obtained at all observable toroidal positions even when viewing the limiter and antennae.

The temporal evolution shown in Figs. 1 and 2 is qualitatively similar to purely ohmic discharges in which the density is increased either by strong puffing of deuterium or by the injection of light impurities. The initial dip in the line-integrated H_α emission in all three cases (rf, puffing, impurity injection) seems to be associated with the initial broadening of the electron density profile.

At lower values of I_p, the density increase is smaller and even appears to vanish if $I_p \sim 20$ kA. However, an overall decrease in particle confinement at these low currents makes interpretation of the results difficult.

III. INFLUENCE OF ALFVEN WAVE SPECTRUM. In Fig. 3 we show the final electron density as a function of the target density for both hydrogen and deuterium discharges with 100 kW of rf power. The curves show regions of apparent re-

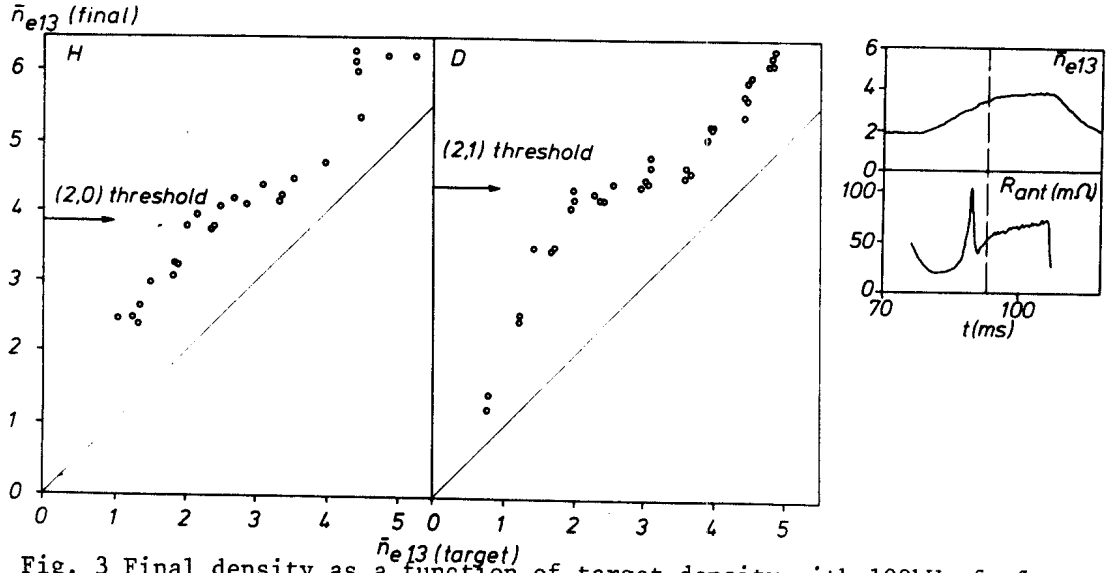

Fig. 3 Final density as a function of target density with 100kW of rf. Inset: Discontinuous behaviour at (2,0) threshold in hydrogen

duced increase ($\bar{n}_e$(final) ~ 4 x 10^{13} cm^{-3} in hydrogen and 4.5 x 10^{13} cm^{-3} in deuterium). This corresponds to discharges which display a discontinuity in the density rise[3] when a new resonance surface appears in the centre of the plasma as shown as an inset in Fig. 3. Apart from these discontinuities, the density rise is normally linear with rf power. This has been verified by using subsets of our 8 antennae to couple equivalent powers with different antenna currents giving the same density increase.

Further evidence of the effect of the Alfvén wave spectrum is given in Fig. 4 where we have varied the antenna phasings to change the dominant toroidal wavenumbers in the excited spectrum. For the same power delivered the density increase is greatest for the N = 4 phasing which is known to couple poorly to central resonant surfaces at this density. Similarly the n = 2 surfaces tend to be more central than the n = 1 yet the N = 1 phasing produces the greater rise in density. It is tempting to link the density rise with a phenomenon that is reduced in importance when central power deposition increases.

IV. PARTICLE CONFINEMENT RECYCLING AND IMPURITIES. We can write the global particle balance equation as:

$$dN/dt = S_H + S_Z - N/\tau_p \qquad (1)$$

where N is the total number of electrons in the discharge, τ_p is the global particle confinement time, and S_H, S_Z represent the ionisation of hydrogen and impurity atoms respectively. In general $S_H = \phi + RN/\tau_p$ where ϕ is the additional source of neutrals from the gas valve and R is the recycling coefficient (representing both back-scattering and de-trapping). Under conditions where ϕ is zero or constant there are three possible causes for a rise in electron density, each of which will be considered in turn.

(a) An increase in S_H due to greater recycling. Integration of the H_α profile suggests that any increase in S_H is commensurate with the overall rise in electron density. Unlike ICRF heating experiments[1] we have never observed any significant increase in neutral efflux. A deuterium discharge fired after a long sequence of hydrogen discharges (and vice-versa) has been used to elucidate further the recycling processes[4]. The ratio of the line-

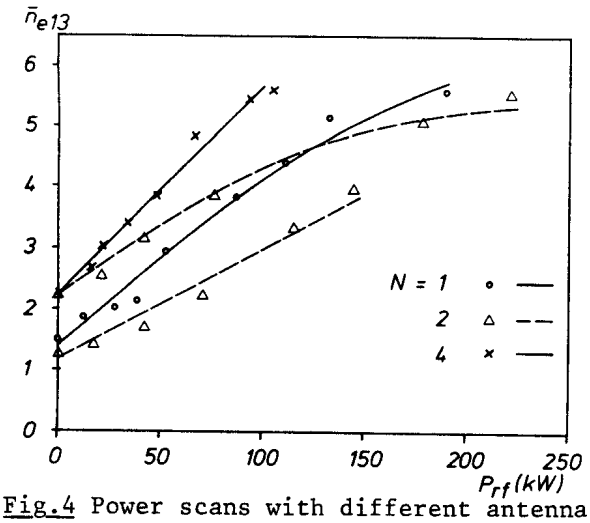

Fig.4 Power scans with different antenna phasings in deuterium discharges

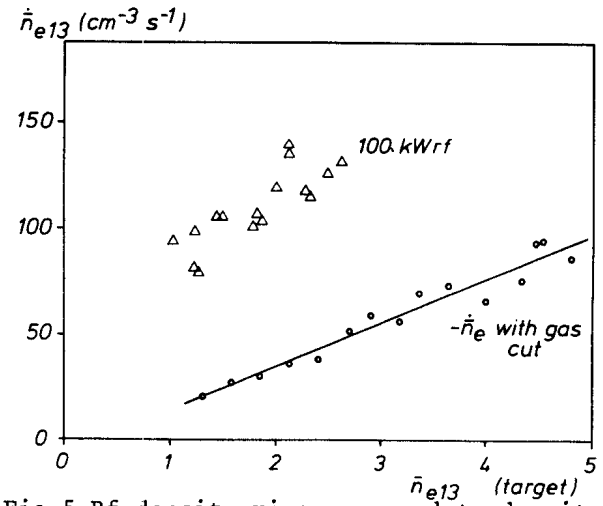

Fig.5 Rf density rise compared to density decrease obtained with gas cut and no rf

integrated emissions of H_α and D_α measured by a Fabry-Perot spectrometer did not change significantly during the rf pulse, indicating that recycling is not substantially modified.

(b) An increase in S_Z due to either a greater flux of impurities or a change in the profiles of temperature and density. As the plasma purity has been improved by successive modifications to limiter design and material and antenna design and materials the density rise has persisted and even seems to be greatest under the cleanest conditions. This argues against the ionisation of impurities as the source of the density rise. Radiated power profiles and simulations indicate that for the discharge shown in Fig. 1 the low-Z and metal impurity concentrations increase from 2.5% and 0.1% to 3.2% and 0.18% respectively. The central Z_{eff} and A_{eff} rise from 2.7 and 1.2 to 3.3 and 1.3 respectively in agreement with measured values (the effective mass A_{eff} can be estimated from the frequencies of the global eigenmodes that appear in the antenna spectrum). The increase in impurity concentration can at most account for 20% of the observed central density rise.

(c) Improved particle confinement. If τ_p becomes infinite, equation (1) gives an upper limit to dN/dt. In Fig. 5 we plot the initial value of $\dot{\bar{n}}_e$ against the target density for the series of discharges shown in Fig. 2. Also shown in Fig. 5 are the results of an experiment without rf in which we cut the external source ϕ. Equation (1) shows that the instantaneous decrease in dN/dt will be equal to the above limit. Even with 100 kW of rf the discharges in Fig. 5 exceed this limit by a considerable factor, pointing to the limitations of a simplistic model.

V. CONCLUSION. It seems that neither improved recycling nor increased impurity concentrations can explain the observed increases in density. If the particle balance is represented as the difference between an inward and outward flux, as is suggested by many experimental results, then the limit on dN/dt is much greater than that predicted by eqn (1). The rf power could act to perturb the balance by either suppressing one of the loss terms contributing to the outward flux or by increasing the inward pinch velocity. In this model it is easier to envisage the spectrum related effects as discussed in section 3.

Acknowledgements. We recognize the assistance of the whole TCA team in this work and the support of Professor F. Troyon and A. Heym. The work was partially supported by the Fonds National Suisse.

References

[1] J. Hosea et al., in Heating in Toroidal Plasmas (Proc. 4th Int. Symp., Rome, 1984) Vol. I, 261.
[2] K.-I. Chen et al., ibid, 680.
[3] K. Appert et al., ibid, 171.
[4] G.M. McCracken et al., Nucl. Fusion 18 (1978) 35.

WAVE STUDIES IN THE SCRAPE-OFF LAYER OF TCA DURING ALFVEN WAVE HEATING

Ch. Hollenstein, F. Hofmann, F.B. Marcus, Y. Martin and W. Simm
Centre de Recherches en Physique des Plasmas
Association Euratom - Confédération Suisse
Ecole Polytechnique Fédérale de Lausanne
21, Av. des Bains, CH-1007 Lausanne, Switzerland

I. INTRODUCTION. In previous studies of the scrape-off layer[1] in tokamaks, the emphasis was on the measurements and interpretation of basic plasma parameters. Recent studies tried to characterise the turbulent state of the scrape-off layer[2,3]. These studies mostly apply to the ohmic heating phase only.

In the TCA tokamak extensive studies of the boundary layer have been performed during Alfvén wave heating. The results have shown that the scrape-off plasma becomes non-maxwellian during rf-heating[4]. Since the antenna is in direct contact with the edge plasma, it may excite various electrostatic waves in the scrape-off layer.

II. EXPERIMENTS. The operating parameters of TCA are $R = 0.61$ m, $a = 0.18$ m and $B \leq 15$kG. For these investigations, reproducible shots at $q \approx 3.3$ in D_2 and H_2 were studied. The rf frequency was fixed at 2.5 MHz and rf powers at around 100 kW were delivered to the plasma.

Movable Langmuir probes were located in the equitorial plane of the TCA vacuum vessel, opposite to the limiter[4]. The different probes were operated either in the ion saturation regime ($V \approx -120$ V), or the floating potential regime or in the grounded mode. This latter mode was used to minimize direct rf-pick up. The fluctuating probe currents in the ion saturation mode and grounded mode were measured by a current probe with a frequency response up to 50 MHz. The floating potential fluctuations were detected by an isolation amplifier with a frequency response up to 20 MHz. The detected signals are digitized by 8 bit CAMAC transient recorders with a sampling frequency up to 32 MHz.

Raw data of the rf current flowing in the grounded Langmuir probe and of the floating potential versus time during Alfvén wave heating are presented in Fig. 1. Beside fluctuations at the driving rf frequency and its harmonics, strong low frequency modulations occur. A typical autospectrum of the rf current is shown in Fig. 2. The floating potential data (Fig. 1b) show the appearance of large narrow spikes at the same repetition frequency as the rf. These rapid potential changes can reach several tens of Volts. The amplitudes of the rf current and of the floating potential fluctuations depend on the

probe position, the rf power and also on the particular heating scenario. A study of the radial behaviour of the potential fluctuations shows that the fluctuations are large at the antenna position. At 1 cm in front of the antenna location, the fluctuations pass through a minimum before steadily increasing towards the limiter position. The rf currents show a different behaviour. At the antenna location, the rf currents are small; they reach a local plateau 1 cm in front of the antenna before continuing to increase towards the limiter.

Correlation techniques[5] have been applied to two simple Langmuir probes spaced at 0.5 cm in the poloidal direction. The coherence obtained from these probes, operated in the grounded mode, is shown in Fig. 3. The coherence reaches nearly unity at the rf-frequency and its harmonics. An asymmetric broadening around the central lines is found. These sidebands show considerable coherence. The spread in frequency of these side bands corresponds approximately to the width in frequency of the low-frequency fluctuations. The phase difference between the two probes, obtained from correlation techniques, is presented in Fig. 4. Since the antenna excites waves at the driving frequency, and also at its harmonics, a dispersion relation may be established, supposing that the excited waves at the harmonics belong to the same type of waves. Figure 4 shows that the phase and therefore also the k values increase, within the precision of the measurements, linearly with frequency, thus indicating a dispersion relation of the form $\omega = v_{ph}k$.

The phase velocity is found to be of the order of 2×10^7 cm/sec. Figure 5 shows that this phase velocity stays constant throughout the scrape-off layer. The phase velocity of the wave in the sidebands is found to be on the order of 10^5 cm/s, the same as the phase velocity of the low-frequency fluctuations.

Correlation techniques have also been applied to the rf current and the detected potential fluctuations. Potential and rf current fluctuations were found to be out of phase at the driving frequency and its harmonics. A change in phase is observed at the antenna location.

In TCA, as in other tokamaks, high-level low-frequency fluctuations are seen in the scrape-off layer. Beside the fact that the antenna excites electrostatic waves, it is of interest whether low frequency waves are influenced by the presence of rf power. The autospectrum of a probe in the ion saturation mode is shown in Fig. 6. During the rf phase, the frequency behaviour is similar to that observed during the OH phase. In both cases the coherence can be as high as 0.8 (Fig. 7). The calculated phases are shown in Fig. 8. During the OH and rf phase, the phases increase approximately linearly with frequency. However, the direction of wave propagation reversed during Alfvén wave heating. Figure 9 shows the phase velocity as a function of the probe position within the boundary layer. The velocity during OH remains rather constant. At 5 mm behind the limiter position, measurements indicate that the phase velocity may be reversed outside the limiter position as observed in other tokamaks[3]. During Alfvén wave heating the localized reversal of the

direction of wave propagation is found to be accompanied by a broadening of the k spectrum S(k). The spectral index α ($S(k) \sim k^{-\alpha}$) drops in the region of reversal from values between 2 and 3 down to about 1.

III. CONCLUSION. The present study shows that the antenna used for auxiliary heating excites electrostatic waves in the scrape-off layer. At present state identification of the launched wave has not been possible. Also the wave excitation mechanism and possible nonlinear processes have to be studied in future. Low frequency fluctuations are strongly affected by the rf. The high level spikes found on the potential fluctuations may play a key role in antenna-plasma interaction, for example in impurity generation.

Acknowledgement. We wish to thank the whole TCA team for their excellent support. Also, the great encouragement from Professor F. Troyon is highly recognized. The present work was partially supported by the Swiss National Science Foundation.

References

[1] S.J. Zweben and R.J. Taylor, Nucl. Fusion 23 (1983) 513.
[2] S.J. Zweben and R.W. Gould, Nucl. Fusion 23 (1983) 1625.
[3] Ch. Ritz et al., Phys. Fluids 27 (1984) 2957.
[4] A. de Chambrier et al., J. Nucl. Mat. 128 & 129 (1984) 310.
[5] D.E. Smith et al., IEEE Plasma Science PS-2 (1974) 261.

Figure Captions

Fig. 1 a) Rf current fluctuations

Fig. 1 b) Floating potential fluctuations

Fig. 2 Autospectrum of rf current

Fig. 3 Coherence

Fig. 4 Phase

Fig. 5 Phase velocity in function of the probe position in the scrape-off layer

Fig. 6 Autospectrum of ion saturation current

Fig. 7 Coherence during OH and rf heating

Fig. 8 Phase during OH and rf heating

Fig. 9 Phase velocity in function of the probe position during OH and rf heating

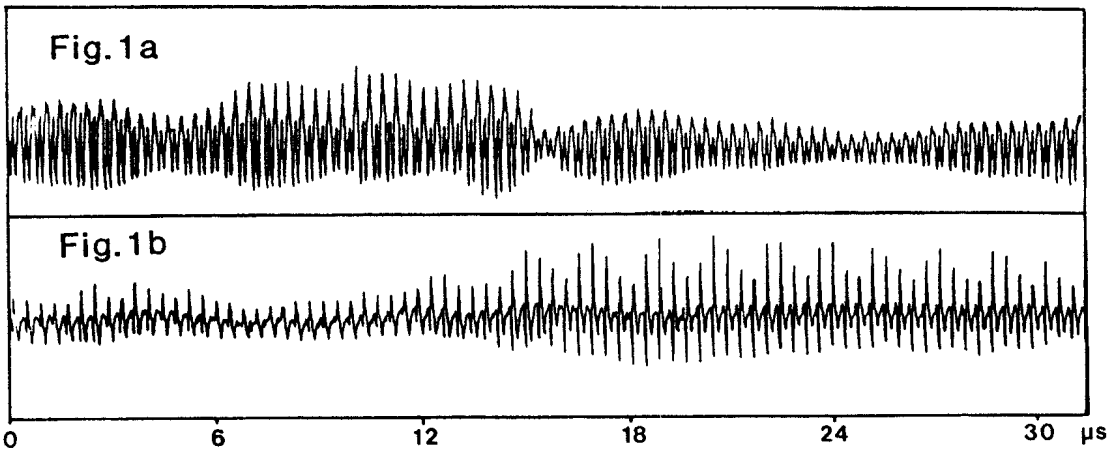

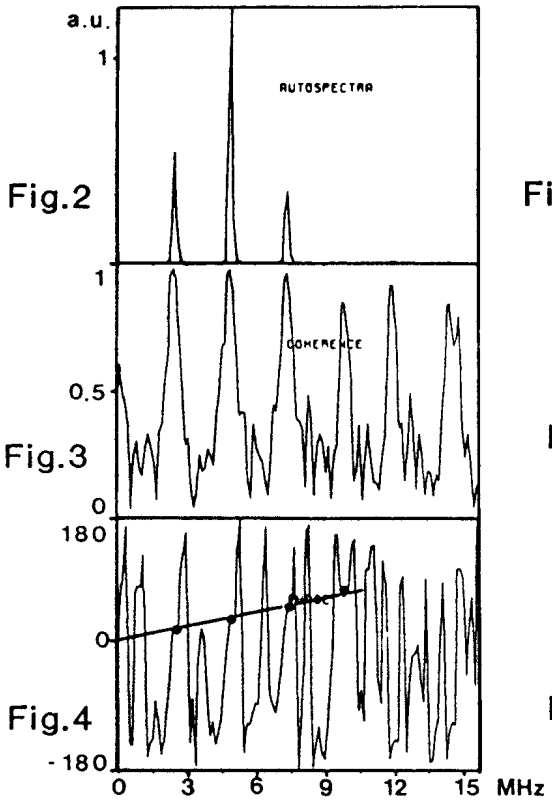

Fig.2

Fig.3

Fig.4

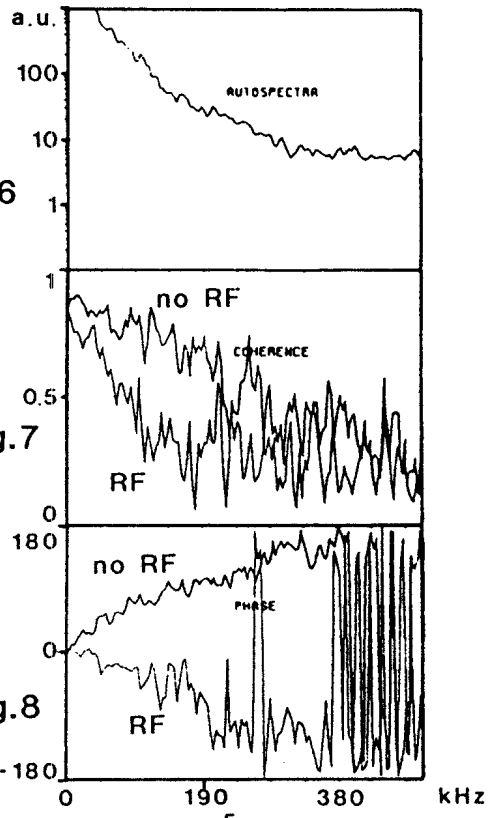

Fig.6

Fig.7

Fig.8

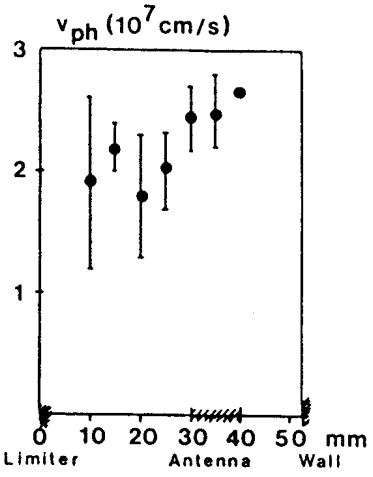

Fig.5

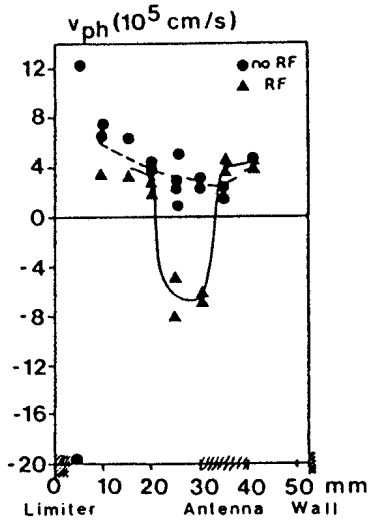

Fig.9

TOWARDS A BETTER UNDERSTANDING OF IMPURITIES IN TCA

B. Joye, J.B. Lister, F.B. Marcus and S. Nowak*
Centre de Recherches en Physique des Plasmas
Association Euratom - Confédération Suisse
Ecole Polytechnique Fédérale de Lausanne
21, Av. des Bains, CH-1007 Lausanne, Switzerland

* Institut de Physique, Université de Fribourg, Switzerland

Abstract. The behaviour of impurities during the Alfvén Wave Heating pulse is still being studied. We show that the impurity increase is independent of the number of active antennae, and depends only on the rf power delivered. The time development of the radiated power profile is discussed, and indicates propagation delay and a final stationary state. Finally, we discuss spectroscopic measurements apparently incompatible with these other data.

I. THE RADIATED POWER PROFILE. The behaviour of the radiated power profile in ohmically heated discharges has been discussed[1]. The initial rf experiments on TCA showed a large impurity increase, which has been reduced to an acceptably low level[2]. We present in Fig. 1 the time-development of the local radiated power loss as a function of radius. The outer radii increase promptly when the 180 kW rf pulse is applied. The radiated power on axis does not increase for some 13 msec, although the central electron density starts rising promptly. This indicates that even with an increasing electron density the highly radiating species in the centre are extremely dilute in the target plasma, and their radiative loss is immeasurably small. The delay is therefore attributed to the propagation time of new heavy impurities, which enter the plasma when the rf is applied. The accumulation of heavy impurities already present before the rf pulse would not therefore be indicated by this temporal behaviour. Towards the end of the 40 msec rf pulse shown in Fig. 1 the radiated power loss on axis stops increasing and for the last 5-10 msec the radiated power is virtually stationary at all radii. This again shows that the new impurities do not increase indefinitely, but a new balance is established after an initial transient rise. If we write the impurity transport as $\Gamma = -D\nabla n + V_{in}\, nr/a$, then we obtain $V_{in} \sim 800\text{-}1200$ cm sec^{-1} for the heavy impurities.

II. DIFFERENT ANTENNA GROUPS. The TCA antenna system comprises eight antenna groups which can be fed separately. We have carried out experiments using different numbers of antennae, as a function of power. Figure 2 shows the increases of total and central radiated power, plasma resistance and the intensity of the SiIII line (1206.5 Å) as the rf power is increased.

Silicon carbide is used as the limiter coating. The relative antenna currents are shown in the figure and we see that over a large range of antenna currents/voltages the impurity increase depends only on the total delivered rf power, for a given target plasma. As a result of these indications, we do not relate the impurity production to effects which are local to the antenna structure, but rather to a change brought about by the total delivered rf power. At present the metallic pollution of the limiters coupled with a change in the scrape-off layer during rf[3] is considered to be one of the most likely origins.

III. SPECTROSCOPIC MEASUREMENTS. The waveform of the SiIII line intensity during one discharge is shown in Fig. 3, together with the antenna loading curve which it accurately reflects. The mechanism relating the two is not yet identified. However, it is not directly proportional to the total rf power or to the antenna current, also shown in Fig. 3. Nor is it one of the rf wavefields measured at the plasma edge, or the total rf wavefield. The increase in the SiIII line is not considered to be only an influx measurement. This "peak reflection" exhibits itself in most low-Z edge lines observed in the VUV part of the spectrum, but less so in the visible spectrum in which few data were taken. It is not considered to be a temperature effect at the emitting radius, as no indication of this effect is seen on the Soft X-ray signals near the plasma edge. We hypothesise that the edge line intensities at the plasma edge may be altered by a non-Maxwellian electron velocity distribution in the outer region of the plasma, similar to that measured in the edge plasma[3].

A study of the core-line intensities has also been carried out, and Fig. 4 shows the intensities of the lines FEXVIII, FEXIX, FEXXI and TiXIX. Apart from their strong increase, the most noticeable feature is their prompt response to the rf, starting to rise in less than 1 msec. The density rise cannot explain this since the sensitivity of these core lines to an increasing density is generally much weaker than linear[4], and the density only increases by a factor of 40% in the discharge shown. The increase cannot be attributed to the time variation of the temperature which is not much higher at the end of the full 30 msec rf pulse. New impurities cannot be the cause since these lines radiate near the plasma centre, and firstly there is the inward propagation delay, shown in the first section, and secondly there is the burn-through delay to the higher ionised states. A further observation is the appearance of a weak "peak reflection" similar to the edge lines on the TiXIX waveform. None of the mentioned effects (except Te, already discounted) could produce such a temporally sharp response. We note that the observation of the spectroscopic line intensities, without detailed bolometric measurements, would have led us to an imcompatible conclusion, namely strong axial accumulation of the impurities already in the plasma.

Acknowledgements. We recognize the help of the whole TCA team and the support of Professor F. Troyon and A. Heym. The work was partly funded by the Fonds National Suisse.

References

[1] B. Joye et al., paper presented at this conference.
[2] A. de Chambrier et al., Proc. X Int. Conf. IAEA, London (1985) 531.
[3] A. de Chambrier et al., J. Nucl. Mater. 128 (1984) 310.
[4] J.D. Lawson et al., J. Phys. B14 (1981) 929.

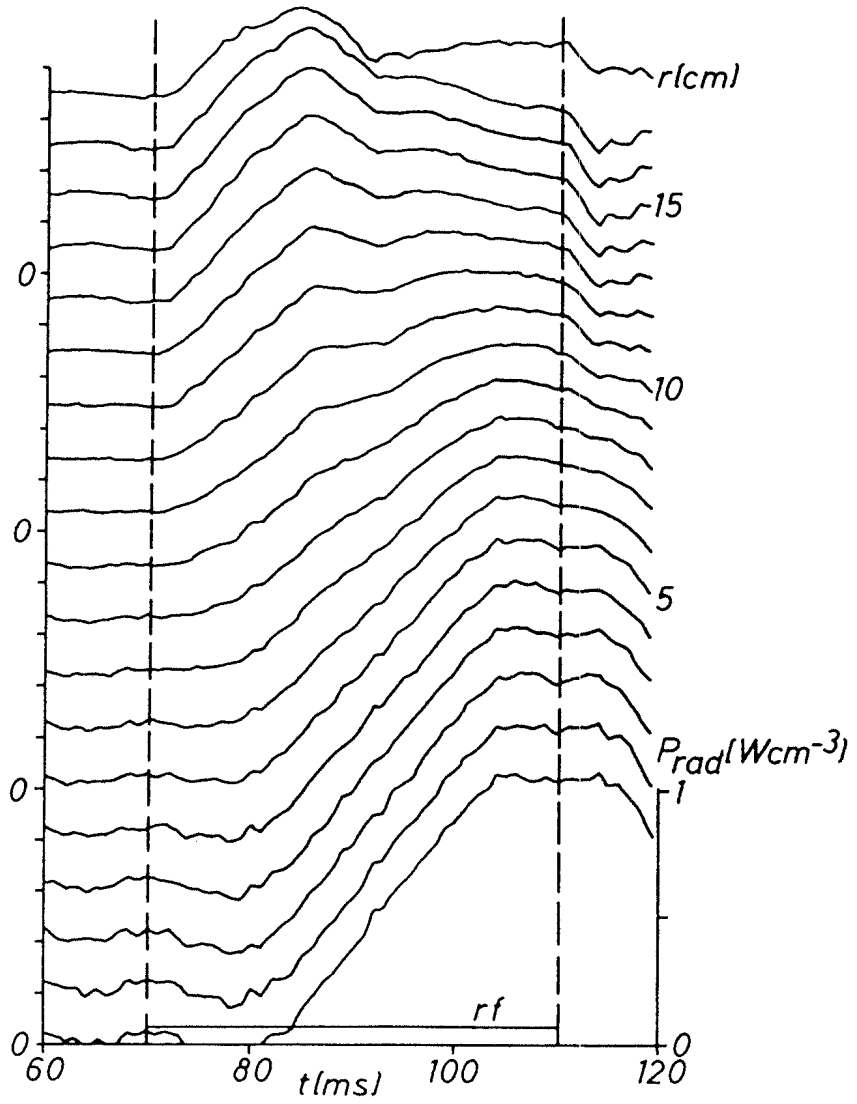

Fig. 1: The temporal evolution of the radiated power loss at different radii during the rf pulse.

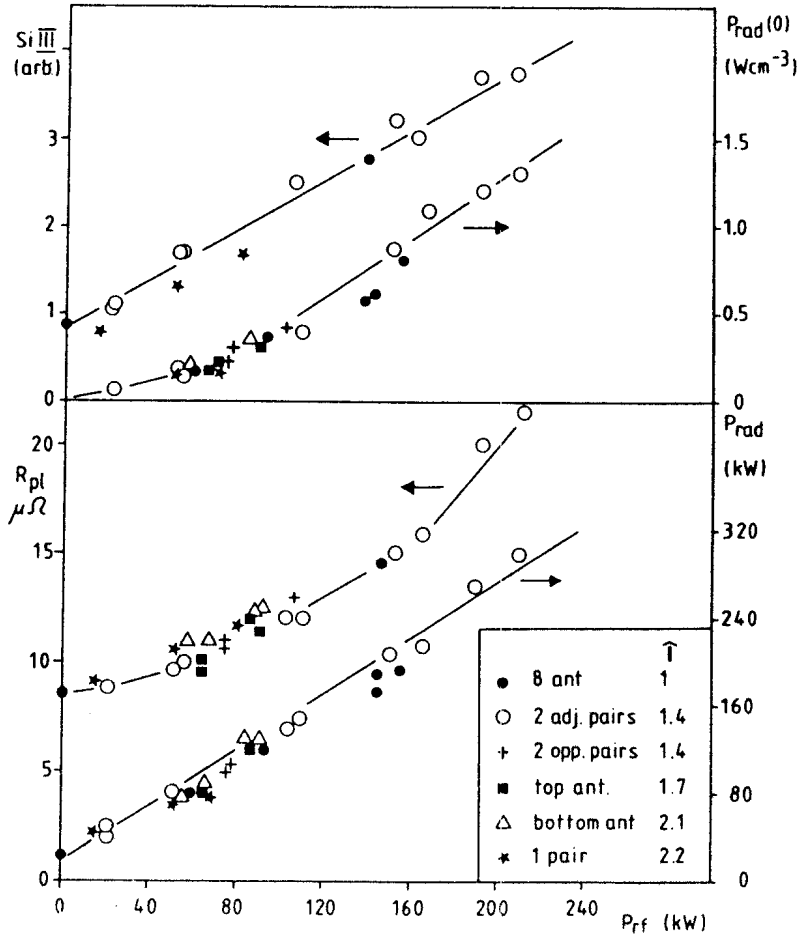

Fig. 2: The increase in the radiated power loss for different groups of antennae.

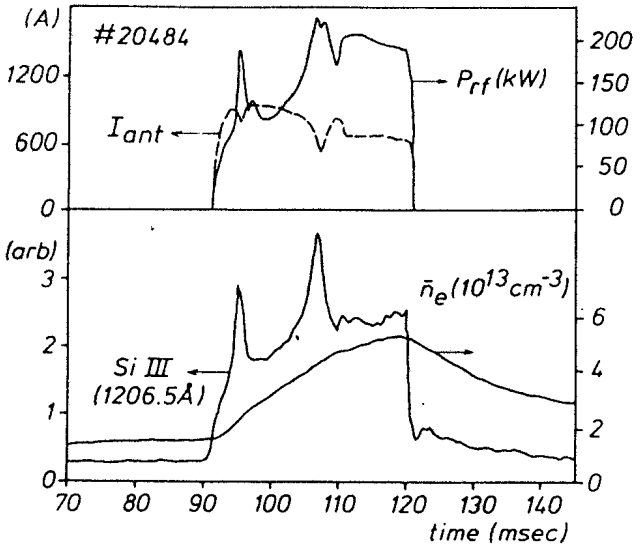

Fig. 3: Time dependence of the SiIII intensity during the rf pulse.

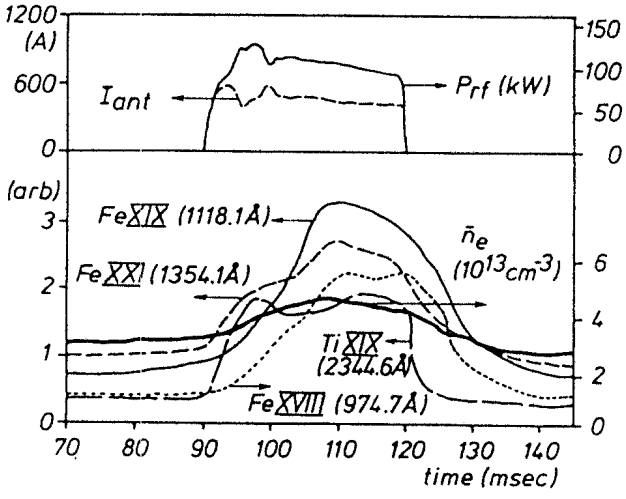

Fig. 4: Time dependence of the core-line intensities during the rf pulse.

THE RADIATED POWER PROFILE UNDER WIDE-RANGING OHMIC CONDITIONS IN THE TCA TOKAMAK

B. Joye, J.B. Lister, Ph. Marmillod, J.-M. Moret, S. Nowak+
Centre de Recherches en Physique des Plasmas
Association Euratom - Confédération Suisse
Ecole Polytechnique Fédérale de Lausanne
21, Av. des Bains, CH-1007 Lausanne / Switzerland

+ University of Fribourg, Physics Departement
Pérolles, CH-1700 Fribourg / Switzerland

Introduction

A multichannel radiation bolometer with 16 detectors [1] has recently been commissioned on the TCA tokamak (R,a = .6,.18m).A pinhole camera design allows the simultaneous view of 16 spatial chords covering an entire vertical plasma cross-section. The radiated power profile of a tokamak pulse (100 ms flat-top) can be obtained with a time resolution of about 1 msec. The detection limit corresponds to about 10 mW/cm^3 after Abel-inversion.

A detailed study of the radiated power profile has been carried out for ohmically heated discharges. Experiments were performed using density and current programming with n_{eo} = (0.15 - 1.05)$\cdot 10^{14}$ cm^{-3} and I_p = 20 - 125 kA at three different magnetic fields (0.78 T, 1.16 T, 1.51 T) thus covering the entire operation range of the TCA tokamak for $q_a > 3$. In all of the conditions the density was increased until the disruption limit was met. All of the parameters were measured at the time of the Thomson T_{eo} measurement. Combining the radiated power profile with the data from an 8-channel FIR-interferometer allowed an estimation of the impurity concentrations. Assuming coronal equilibrium an attempt was then made to model the radiation profile. Particular interest was also invested to a short period before a disruption occurred.

Another set of discharges was dedicated to the study of impurity injection of low-Z gases resulting in a large increase of the electron density. As in the previous case the evolution of the radiated power profile under these conditions was studied and the concentrations of these impurities were compared with calculations assuming coronal equilibrium.

Results

The total radiation loss is dependent mainly on density, being linear with density throughout the entire operation range. Both total and central radiated power roughly follow the density. There is a weak inverse dependence on plasma current as well but no evidence for a strong influence of the toroidal magnetic

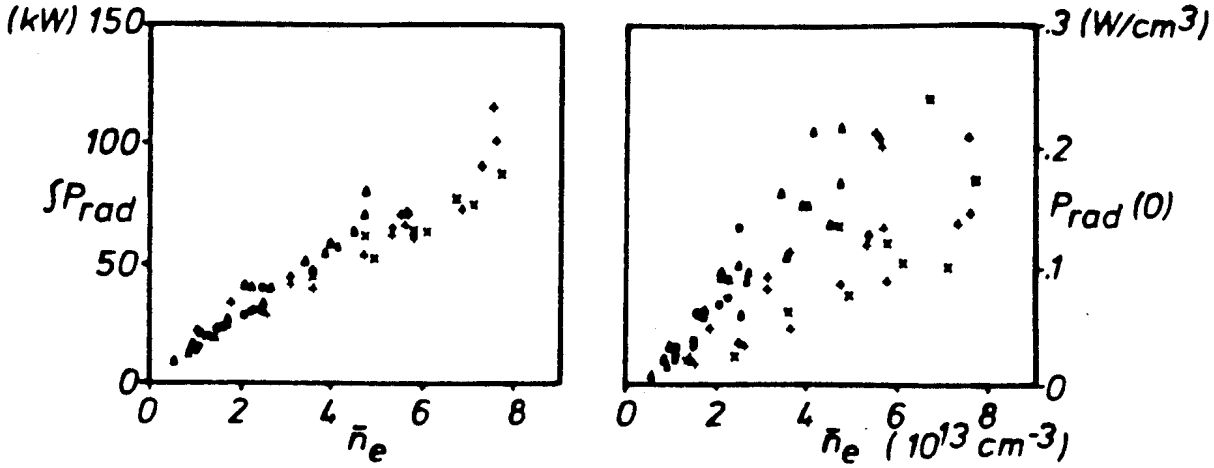

Fig.1 Total and central radiated power as function of electron density for ohmically heated discharges. The symbols correspond to different ranges of plasma current, • - 30 kA, ▲ - 60 kA, + - 100 kA, × - 125 kA.

field. If we consider the central radiated power the same tendencies can be observed with a larger scatter on the experimental data due to the errors introduced by Abel-inversion. These results are summarized in Fig. 1. Comparing the central radiated power with the central ohmic power for non-disruptive discharges results in values of $P_{rad}(0)/P_{oh}(0)$ ranging from 1% to 15%, assuming $q(0) \simeq 1$.

The radiated power profile in the low density, high current corner of the operation diagram is hollow with very little radiation from the plasma axis. As the density is increased no particular change in the shape of the radiation profile can be observed but the level increases linearly with density. For these low q conditions the radiation is probably dominated by low and intermediate Z impurities. As the current decreases the radiated power profile became flatter and eventually slightly peaked on axis. This is consistent with the image of a shrinking current channel together with a decreasing central electron temperature.

Making the usual assumption that P_{rad} is proportional to the product of electron and impurity density [2] with a cooling rate, the impurity concentration can be calculated by dividing the radiated power profile by the electron density profile. The limiter for these discharges was made of carbon with a coating of SiC. Consequently a large signal from Si-lines was observed spectroscopically. Assuming coronal equilibrium Si concentrations were estimated in order to match the central radiated power. Taking the density and temperature values into account the coronal model overestimates the total radiated power by far if only Si is considered. We therefore conclude that several impurities contribute substantially to the radiated power. A small fraction of high-Z impurities, Fe or Ti (both present in the vacuum chamber), accounts for a part of the observed core radiation. Si mostly contributes to the radiation from intermediate plasma

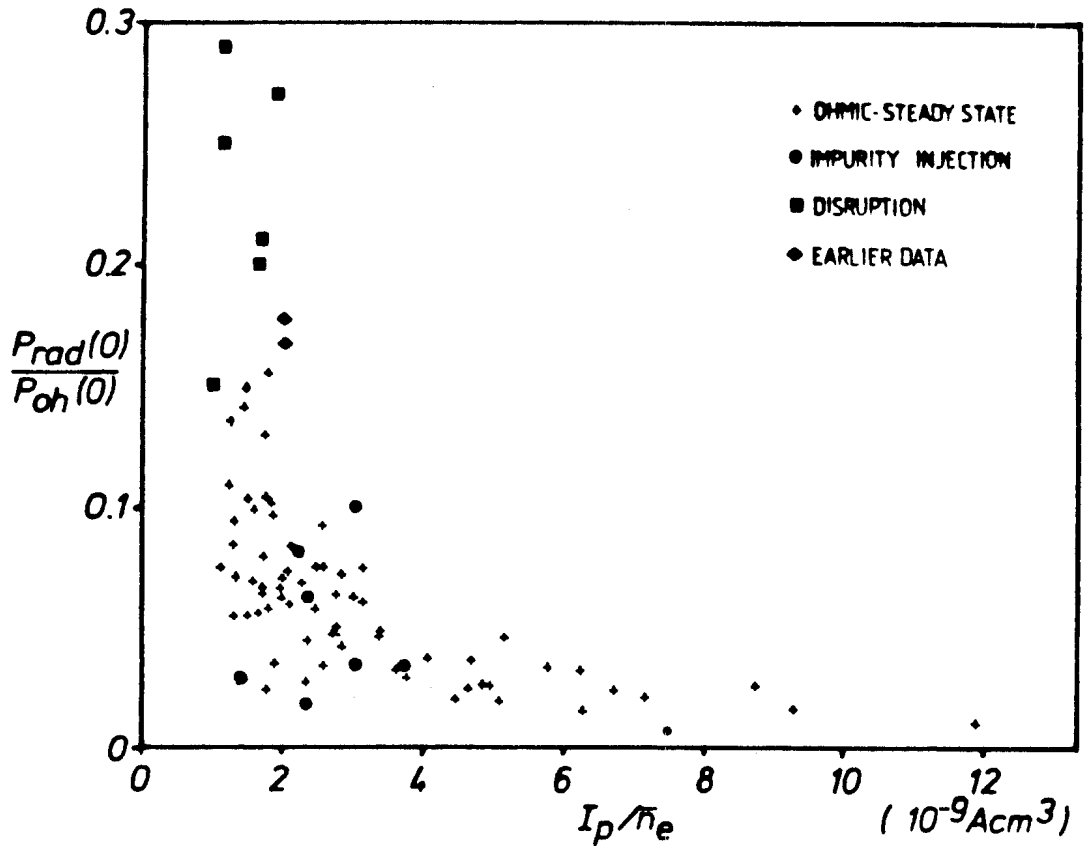

Fig.2 $P_{rad}(0)/P_{oh}(0)$ for different plasma conditions for $q_a > 3$ as function of the operational parameter I_p/n_e.

radii. In order to explain the observed value of Z_{eff} ranging from 1.5 to 3 up to two percent of low-Z impurities (O and C) have to be considered. Carrying out these modeling calculations for all of the conditions shows no large deviations from this picture of a mixture of impurities contributing to the radiated power. As a consequence one should rather concentrate on the impurity density than the concentration. Over all the conditions observed the impurity densities remain fairly unchanged. This again is consistent with the good linearity of the radiated power with electron density. Average impurity densities are $n_m \simeq 0.3\ 10^{11}$ cm^{-3}, $n_{Si} \simeq 1.5 \cdot 10^{11}$ and $n_l \simeq 2 \cdot 10^{11}$ cm^{-3}. The coronal model thus gives a consistent picture of the radiated power profile although the measured profile does not show all of the spatial details.

During these experiments the electron density was increased until a disruption occured. The radiated power profile was studied in detail for evidence of its possible influence on the disruption. Looking at the time evolution of the radiated power profile a few msec before a disruption showed no evidence of a precursor to the disruption. In particular no strong peaking or asymmetry of the bolometer profile was observed. We therefore conclude that there is no evidence for the radiation being the primary cause for the disruption even if the level of radiation is high before the disruption. Discharges were observed in ear-

lier experiments [3] where a similarly large radiated power was not followed by a disruption. This is again consistent with the fact that impurity densities remain fairly unchanged with changing plasma conditions so it seems that there is no particular accumulation of impurities which could invoke a radiation level large enough to destabilize thermally the plasma column. Once the disruption has occured the radiated power strongly peaks on axis due to the cooling and fast current narrowing. The total radiation loss observed cannot be explained by the content of the kinetic energy alone. A considerable amount of stored magnetic energy is lost through radiation as well, e.g. $W_{rad} \simeq 2.0$ kJ, $W_{kin} \simeq 1.3$ kJ and $W_{mag,int} \simeq 4.4$ kJ.

Impurity puffing of various low-Z gases (He, Ne, N_2 and O_2) was carried out into hydrogen discharges resulting in an increase in density of up to 250%. The radiation profile for these experiments again followed the density, being hollow throughout the pulse, indicating that low-Z impurities account for the increase in total radiation. No increase in central radiated power was observed, therefore the concentration of heavy impurities does not change with low-Z impurity puffing. The coronal model which was applied to these experiments could well explain the increase in radiation by the incoming impurities. Before injection the radiation is likely to be dominated by Si-lines. During injection the radiation can be explained by the same Si-density and a reasonable concentration of the injected impurity. Thus the radiation profile can be described by a rather unchanged density of intrinsic impurities in combination with a certain amount of the injected impurity which is consistent with the case discussed above.

In Fig. 2 $P_{rad}(0)/P_{oh}(0)$ is plotted for the different experimental series covered by this paper. For this parameter values up to 0.5 were observed in earlier experiments not being followed by a disruption [3].

Conclusion

The modeling of the radiated power loss carried out for various ohmic conditions and impurity injection led to a consistent picture of the impurity composition of the TCA tokamak plasma. Impurities and the associated radiated power are not a severe problem in the present clean conditions.

Acknowlegements

We recognize the assistance of the whole TCA team in this work and the support of Prof. F. Troyon and A. Heym. The work was partly supported by the Fonds National Suisse.

References

[1] H. Jaeckel et al., Proc. DPG, Munich, 1978
[2] D. Post et al.,Atomic Data and Nucl.Data Tables 20(1977) 397
[3] F. Hofmann et al., Lausanne Report LRP 229/83

STUDIES OF THE BROADBAND MAGNETIC FLUCTUATIONS IN THE TCA TOKAMAK

M.L. Sawley, A. Pochelon and R. Keller
Centre de Recherches en Physique des Plasmas
Association Euratom - Confédération Suisse
Ecole Polytechnique Fédérale de Lausanne
21, Av. des Bains, CH-1007 Lausanne, Switzerland

There is at present a large interest in the study of microscopic fluctuations in an attempt to understand the observed anomalous transport in tokamak plasmas[1]. Recent preliminary investigations on several tokamaks have shown a strong relation between the level of broadband magnetic fluctuations at the plasma edge and the global confinement time. This has been demonstrated both in ohmic (TCA[2], JET[3]) and neutral beam heated (ISX-B[4], D-III[5]) discharges, the level of magnetic fluctuation decreasing with increasing confinement time. It is important to note that no such relation has been found for low temperature tokamaks[6,7].

To date there has not been a detailed study of how the fluctuation amplitude varies over the possible wide range of tokamak operational parameters. In the present paper we report on such a study, undertaken in the ohmic phase of TCA. The main TCA parameters are $R = 61$ cm, $a = 18$ cm, $B_\phi < 1.51$ T, $I_p < 175$ kA with a current flat-top of $\lesssim 150$ ms, yielding $\bar{n}_e < 10^{14}$ cm^{-3} and $T_e < 1$ keV. The fluctuating field is detected with wide bandwidth, triple (measuring $\tilde{b}_r$, $\tilde{b}_\theta$ and $\tilde{b}_\phi$) magnetic probes. The probes are placed in the shadow of the limiters, since internal measurements are not possible in TCA. The results described here were obtained from a probe situated in the equatorial plane. Spectral information of the broadband fluctuating field which is observed at frequencies above that of the Mirnov oscillations ($\sim$ 10 kHz) was obtained by passing the probe signal through a series of 8 adjacent half-octave passive bandpass filters, covering the frequency range of 40 - 660 kHz.

As has been observed on other tokamaks, it was found that b_r and b_θ are similar in amplitude. However, by careful alignment of the rotatable probe it was possible to determine that the fluctuating field is plane-polarized normal ($\pm 2^\circ$) to the toroidal direction. This result was found over the entire fluctuation spectrum for the wide range of $3.3 < q(a) < 7.3$ considered. Hence, we find that the broadband magnetic fluctuations are confined to a plane normal to the toroidal magnetic field and <u>not</u> to the total magnetic field at the probe position.

The fluctuating field has been measured over a large number (> 150) of

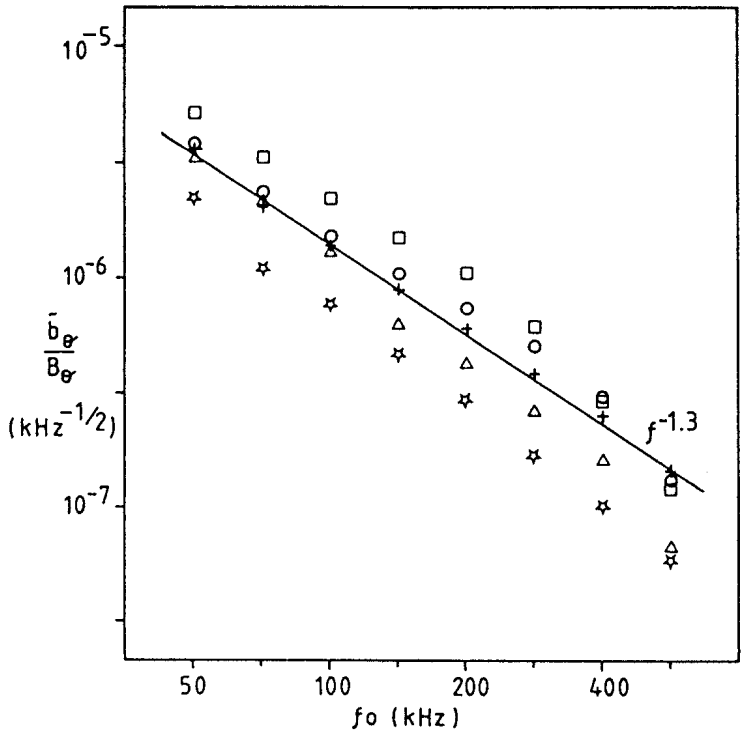

	B_ϕ (T)	q(a)	$\bar{n}_e$ (10^{13} cm^{-3})
△	1.16	3.1	2.5
+	1.16	3.1	1.5
○	1.16	5.5	1.5
□	0.78	5.5	1.5
✡	1.51	3.1	2.5

with $\dot{\bar{n}}_e$, $\dot{\bar{I}}_p \simeq 0$

Figure 1

tokamak discharges spanning the operational regime: B_ϕ = 0.78, 1.16, 1.51 T; $2.6 < q(a) < 15$; and $6 \times 10^{12} < \bar{n}_e < 10^{14}$ cm^{-3}. Deuterium was used as the working gas. All discharges considered had a low level of mode activity with no discernible runaway population. As shown in Fig. 1, the rms value of $\tilde{b}_\theta/B_\theta$ varies as $f^{-1.3\pm0.3}$ over a wide range of operational parameters. Although somewhat different spectra have been measured for extreme values of $\bar{n}_e$ and q(a), taking a single band (that centred around 140 kHz, for example) as representative of the entire spectrum appears nevertheless justified.

Before determining the scaling of the fluctuation amplitude with the various parameters, it is important to gauge its dependence on the rate of change of those parameters that may vary during a tokamak discharge. In Fig. 2

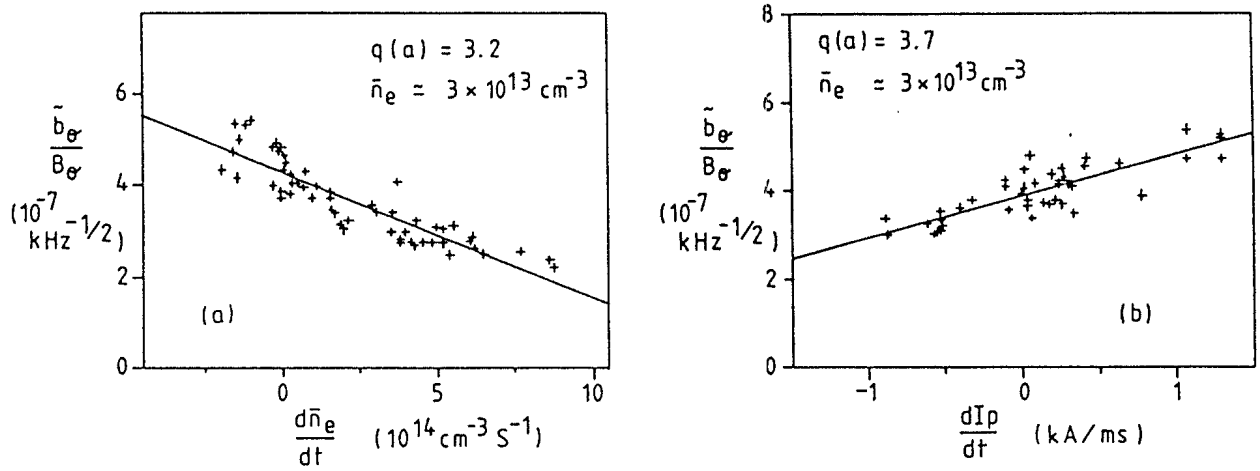

Figure 2

is plotted the rms value of $\tilde{b}_\theta(140\ \text{kHz})/B_\theta$ as a function of (a) $d\bar{n}_e/dt$ and (b) dI_p/dt, keeping all the other parameters constant. It is seen that $\tilde{b}_\theta$ decreases with increasing $\bar{n}_e$ or decreasing I_p. This was found to be true for all values of $\bar{n}_e$ and I_p, although the change in $\tilde{b}_\theta/B_\theta$ with $\dot{\bar{n}}_e$, $\dot{I}_p$ is a function also of $\bar{n}_e$, I_p.

By considering only times in discharges for which $\dot{\bar{n}}_e$ and $\dot{I}_p$ were small, the dependence of the fluctuation amplitude on B_ϕ, I_p and $\bar{n}_e$ was determined. (This was achieved either by a regression analysis of the entire database, or by considering values for which two of these parameters were constant over a range of the third, yielding similar results.) As shown in Fig. 3, it was found that over the entire operational regime $\tilde{b}_\theta(140\ \text{kHz})/B_\theta \propto (B_\phi \bar{n}_e^{1/2})^{-1}$. The normalized fluctuation amplitude, $\tilde{b}_\theta/B_\theta$, was found to depend only very weakly on the value of I_p. It should be noted, however, that the normalization for the fluctuation amplitude is not unique. The most appropriate normalization should, in principle, be determined by the theoretical model with which one is interpreting the experimental data.

It is interesting to note that for the TCA tokamak operating under identical conditions, the energy confinement time, $\tau_E^* = 1.5\ \bar{n}_e k[f_e T_e(o)+f_i T_i(o)]/P_{OH}$ with $f_e = 0.3$, $f_i = 0.5$ is proportional to $B_\phi \bar{n}_e^{1/2}$, as shown in Fig. 4. The reason for the weaker than linear dependence of τ_E^* on $\bar{n}_e$ is attributed to the fact that for the higher values of $\bar{n}_e$ considered in the present wide parametric study, ion neoclassical thermal conduction becomes an important loss channel[2]. The present scaling compares favourably with that determined by considering data from a number of ohmically heated tokamaks with circular plasma cross-section[8].

Comparing the above two experimentally determined scaling laws suggests that the normalized fluctuation amplitude $\tilde{b}_\theta/B_\theta$ scales inversely proportional to the energy confinement time. The present study thus extends the pre-

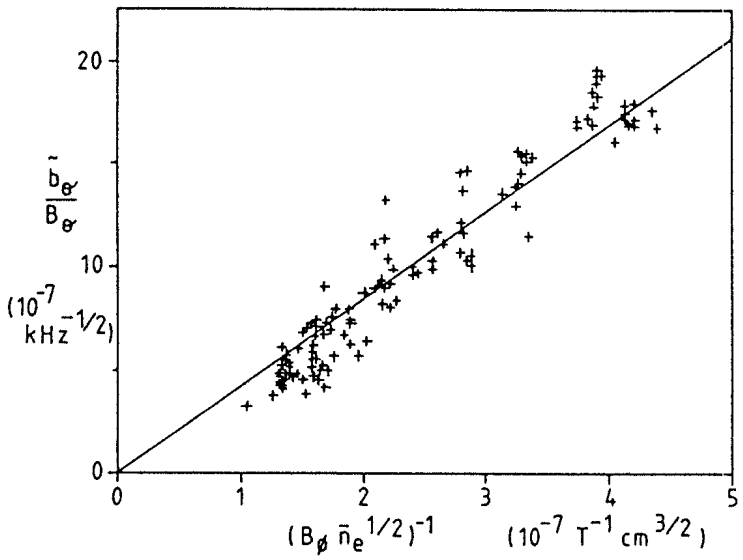

Figure 3

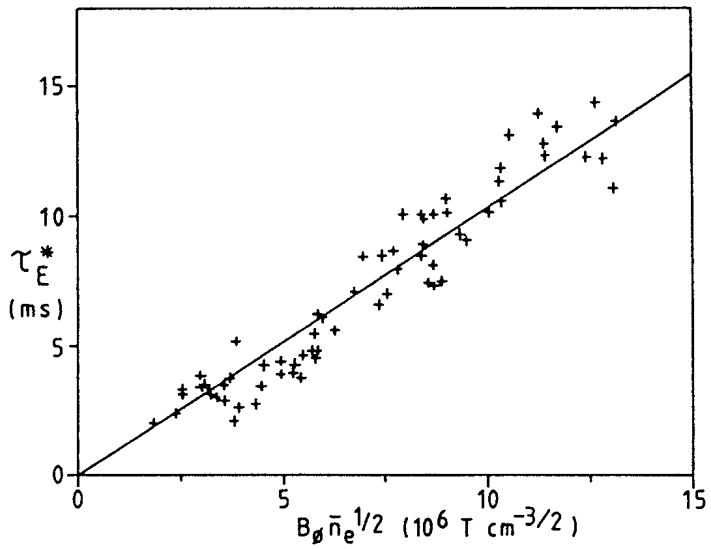

Figure 4

liminary results of magnetic fluctuation scaling obtained to date to a much wider range of tokamak operation, as well as quantifying the dependence on various plasma parameters. In addition, the important role played by the plasma geometry in determining the polarization of the magnetic fluctuations has been shown.

Acknowledgements: The authors gratefully acknowledge the efforts of P.A. Duperrex, Ph. Marmillod and W. Simm towards the present work. They also thank A. de Chambrier, B. Joye, J.B. Lister and J.-M. Moret for making available unpublished experimental data. This work received support from the Fonds National Suisse.

References:

[1] P.C. Liewer, Nucl. Fusion 25, 543 (1985).
[2] P.A. Duperrex et al., Phys. Lett. 106A, 133 (1984).
[3] P.A. Duperrex et al., Paper 98, this conference.
[4] M. Murakami et al., Proc. 10th Int. Conf. Plasma Phys. Controlled Nucl. Fusion, 1, 87 (1985).
[5] E.J. Strait et al., Proc. 11th EPS Conf. Controlled Fusion and Plasma Phys., Aachen, 1, 59 (1983).
[6] S.J. Zweben et al., Phys. Rev. Lett. 42, 1270 (1979).
[7] J.J. Ellis et al., Proc. 10th Int. Conf. Plasma Phys. Controlled Nucl. Fusion 1, 363 (1985).
[8] J. Hugill and J. Sheffield, Nucl. Fusion 18, 15 (1978).

MAGNETIC ACTIVITY DURING INTERNAL DISRUPTIONS IN JET DISCHARGES

P.A. Duperrex*, R. Keller*+, M. Malacarne and A. Pochelon*+

JET Joint Undertaking
Abingdon, OX14 3EA, Great Britain

* on attachment from, + permanent address,
Centre de Recherches en Physique des Plasmas
Association Euratom - Confédération Suisse
Ecole Polytechnique Fédérale de Lausanne
21, Av. des Bains, CH-1007 Lausanne, Switzerland

Abstract. Two new types of magnetic activity have been measured by the internal magnetic coils on a very fast time scale during the thermal relaxation produced by the internal disruption. They indicate a propagation at a wave speed, in addition to the usual thermal diffusion pulse.

I. INTRODUCTION. JET is at present the largest magnetic confinement device. The parameters are $B_\phi \leq 3.45$ T, $I_p \leq 5$ MA, $R = 2.96$ m, $a = 1.25$ m, discharge elongation $b/a < 1.6$ and energy confinement time close to a second.

JET is equipped with 144 magnetic coils distributed in 8 equidistant poloidal planes with 18 coils in each octant. This permits both toroidal and poloidal mode determination. These coils measure the magnetic field component parallel to the vacuum vessel wall (i.e., that principally oriented in the b_θ direction). These coils are protected by a 2.5 mm thick inconel 600 tube which integrates $\dot{b}_\theta$ above 10 kHz. The signal is therefore proportional to $\dot{b}_\theta$ below 10 kHz, whereas above 10 kHz it is proportional to the magnetic field b_θ.

The other diagnostics used are electron cyclotron emission (ECE) in the Fabry-Perot mode, providing the electron temperature evolution on axis, various provisional soft X-ray diodes, viewing horizontally and tangentially through a central chord, the H_α light emission from the limiter, and a reflectometer signal measuring a constant density layer displacement.

II. FAST MAGNETIC PULSE. The first type of observed magnetic activity, which has been called the Gong-mode, takes the form of a fast $\dot{b}_\theta$ pulse, lasting typically 1 ms and having a toroidal mode number $n = 1$. Its transient resembles a strongly-damped ($Q \sim 1$-2) motion, with an oscillation frequency between 2-6 kHz (Fig. 1).

The arrival of the "Gong"-motion at the edge is much in advance of the heat pulse as indicated by the limiter H_α light emission (Fig. 2). It appears in perfect simultaneity with the internal disruption, as measured by

the ECE central electron temperature fall on axis, which has been acquired on the same ADC-unit, with a sampling frequency of up to 40 kHz. During the internal disruption, the electron temperature drop lasts typically 50-200 μsec. The $\dot{b}_\theta$ "Gong" signal measured at the edge sometimes even preceeds the explosive phase of the internal disruption, as exhibited by the rapid fall of T_e on axis. Thus $\dot{b}_\theta$ is capable of revealing the very first phases leading to the explosive process. The radial motion revealed by the reflectometer yields very similar information to the integrated $\dot{b}_\theta$ signal.

The toroidal mode number n, determined by using 4 low field side quasi-equatorial probes and integrating $\dot{b}_\theta$, yields clearly an n = 1 motion, n = 0 and n = 2 components being an order of magnitude smaller. The poloidal distribution is evolutive and strongly asymmetric: the pulse occurs first predominantly on the outside equatorial position (coil 1 and 18, Fig. 3), then progressively "invades" the other poloidal angles. The m-number is seen to evolve rapidly towards higher m's, with typically $3 \lesssim m \lesssim 5$, as determined by the number of poloidal periods. The strong low/high field side asymmetry is of the order of 5 to 10, even with the plasma closer to the probes located near the inner wall than to the probes at the outer wall. One should stress the essentially different character of the "Gong" oscillation compared to the periodically enhanced m = 2, n = 1 island activity at lower frequency sometimes observed around the sawtooth drop[2]. These two activities are often observed to coexist. The helicity of the deformation is measured to be of the same sign than that of the field lines.

The amplitude of the "Gong" motion increases with decreasing q_ψ. It also increases when the sawtooth amplitude is enhanced during rf-heating. Typical b_θ amplitudes are in the range of 10^{-4} Tesla.

The mode structure obviously strongly "remembers" the n = 1, m = -1 helical structure of the q = 1 surface, located close to the core, from where the motion presumably originates. The observation of the n = 1 toroidal mode number can obviously not be explained by an n = 0 rearrangement of the equilibrium. Furthermore, the n number cannot be modified by toroidal and non-circular shape coupling, consistent with the observation. On the contrary, the poloidal modes m are coupled which may explain the various m-number measured, depending on conditions. The very fast transmission from the core to the edge indicates a wave phenomenon. The observed helicity is characteristic of the n > 0 side of the spectrum where the stable MHD-modes are close to zero frequency, i.e. $n + m/q(r) \simeq 0$, with n = 1, q > 0 and n and m of opposite sign. The radial propagation may either originate from the coupling of such a low frequency wave with a fast wave (kink), or may be due to a global MHD-wave[3]. More experimental and theoretical investigations are needed.

III. MAGNETIC BROADBAND ACTIVITY. The level of magnetic broadband turbulence has been shown to be strongly related to electron confinement time both in ohmic discharges[4] and in neutral beam-injected discharges[5].

The b_θ spectrum measured between 10 and 60 kHz shows a $f^{-2\pm0.5}$ depen-

dence, with typical levels of a few 10^{-8} Tesla $kHz^{-1/2}$ at 10 kHz. This level is not sensitive to the amplitude of the m = 2 n = 1 Mirnov activity, except at the very high predisruptive amplitudes, for which it dramatically increases.

After each internal disruption, the magnetic broadband activity (at 15 kHz) exhibits a periodic enhancement of more than a factor 2 in low q (q_ψ < 3) discharges, with a sharp rise less than half a millisecond after the internal disruption (Fig. 4). This increased activity is measured at the edge at a time before the heat pulse has reached the edge, as measured by the periodic H_α-light enhancements. We therefore conclude that confinement properties in the core and magnetic broadband activity are inversely related, and on time scales that seem to reveal a faster than a diffusive propagation.

IV. CONCLUSIONS. We have measured magnetic activity at the edge of the discharge related to the very central q = 1 internal disruption activity. The time scale indicates for both the described activities a wave rather than a solely diffusive propagation. The "Gong"-mode is characterised by n = 1, strong poloidal ballooning-like asymmetries, a step in b_θ with the main frequency component between 2-6 kHz, and the same sign of helicity as the field lines.

Acknowledgements. It is a pleasure to acknowledge stimulating disussions with Professor F. Troyon. L.C. de Kock and G. Tonetti and A.L. Stevens are gratefully achnowledged for making the magnetic measurement available, as well as D. Campbell, R. Gill, A. Hubbard and P.D. Morgan for diagnostics information, and T. Hellsten and K. Appert for valuable discussions.

References:

1. P.A. Duperrex, R. Keller, A. Pochelon and G. Tonetti, SSP Spring Meeting, March 1985, Helvetica Physica Acta 58, 4 (1985).
2. A.W. Morris and D.C. Robinson, private communication (1984).
3. K. Appert, J. Vaclavik and L. Villard, Phys. of Fluids 27 (1984) 432.
4. P.A. Duperrex et al., Phys. Lett. 106A (1984) 133, this Conf. Paper 97.
5. B.A. Carreras et al., Phys. Rev. Lett. 50 (1983) 503.

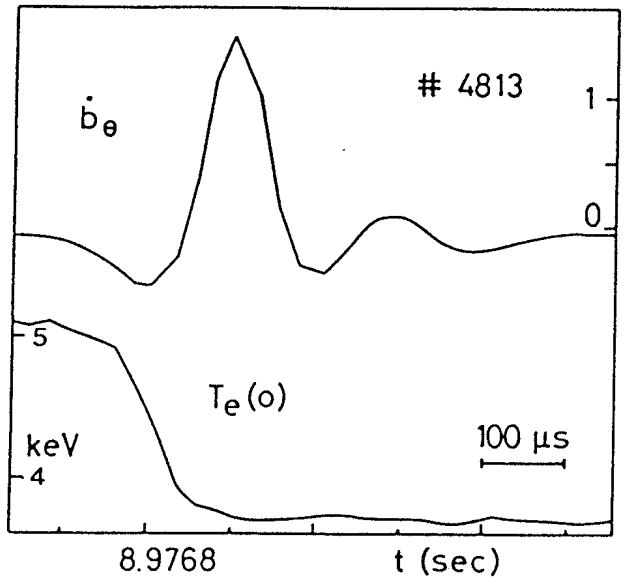

Fig. 1: The "Gong"-mode exhibited by the $\dot{b}_\theta$ signal at the time of the internal disruption, shown together with the central electron temperature drop (ECE)

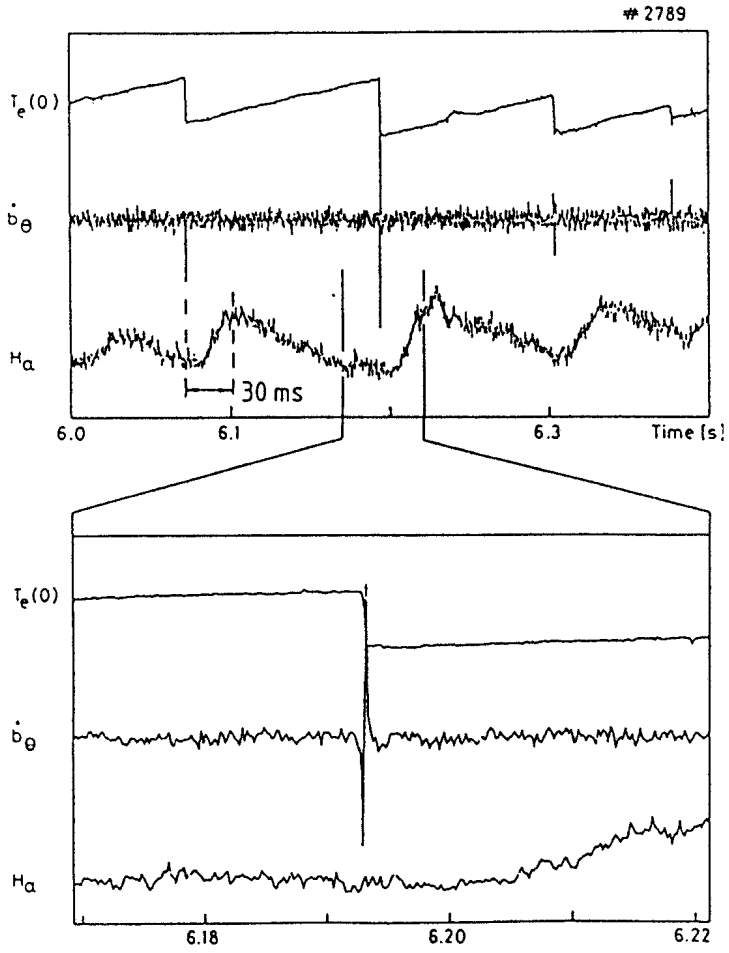

Fig. 2: The internal disruption on T_{eo} $\dot{b}_\theta$ and the heat pulse indicated by the limiter H_α light emission.

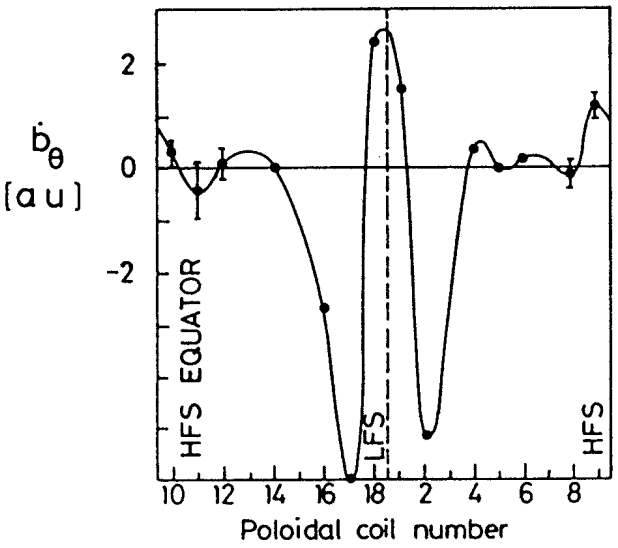

Fig. 3: A poloidal section of the "Gong"-mode, showing the strong asymmetry

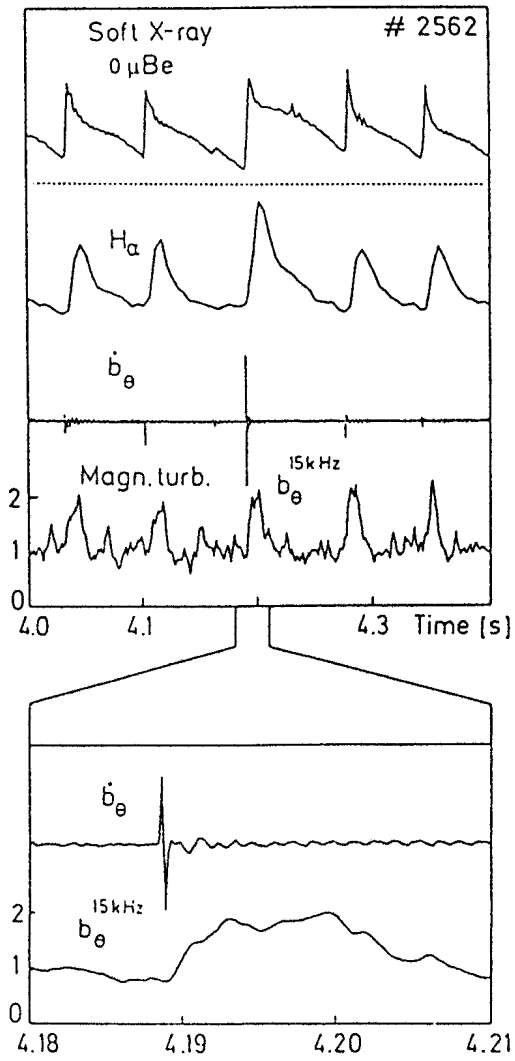

Fig. 4: The magnetic broadband turbulence pulse ($b_\theta^{15\,kHz}$), shown together with soft X-rays, limiter H_α and the "Gong"-mode as a time-marker of the internal disruption.

POSITIONAL STABILITY OF HIGHLY ELONGATED TOKAMAK PLASMA IN A CONDUCTING SHELL

F. Hofmann, F.B. Marcus and A.D. Turnbull

Centre de Recherches en Physique des Plasmas
Association Euratom - Confédération Suisse
Ecole Polytechnique Fédérale de Lausanne
21, Av. des Bains, CH-1007 Lausanne, Switzerland

I. INTRODUCTION. Recent theoretical and experimental results indicate that elongated tokamaks may have considerably higher beta limits than circular ones [1-4]. However, elongated tokamaks are subject to positional instabilities, which must be suppressed by a combination of active and passive stabilization systems, the passive elements being placed "close" to the plasma surface.

When we consider the startup phase of an elongated tokamak, this problem becomes even more difficult: Let us assume that the elongated plasma will be produced by starting with a circular one and then extending the cross-section until it reaches its final shape. In this case, there will be intermediate states which are positionally unstable and which cannot have conducting walls or passive coils everywhere close to the plasma, since room must be left for further expansion. It is clear that, under these circumstances, the startup phase will be critical.

The basic question which we wish to address in this paper is the following: Are there configurations which will ensure positional stability throughout the startup evolution, as the plasma elongation increases up to a value of four, for example.

II. STARTUP SCENARIO. We assume an axisymmetric plasma whose shape evolves from a circle to a vertical race-track with b/a = 4 (Fig. 1). The plasma is surrounded by a conducting shell with rectangular cross-section. During the startup phase, the plasma shape and its position within the shell are adjusted in such a way as to obtain the maximum wall-stabilization effect.

This implies that the shape will always be a race-track with straight lateral boundaries, and the plasma position will be asymmetric with respect to the midplane (Fig. 1). The equilibria shown here were computed with the FBT code [5], assuming $p' = c_p(\varphi+\ell\varphi^2)$, $TT' = c_T(\varphi+\ell\varphi^2)$, where $\varphi = (\psi-\psi_{lim})/(\psi_{axis}-\psi_{lim})$, $c_T/c_p=R_o^2\mu_o((1/\beta)-1)$, $\beta=0.3$ and $\ell= -0.5$. This gives fairly broad current profiles, which are superior for vertical stability, as will be shown below. The plasma current is assumed to increase with elongation such that q_ψ remains constant at the plasma-vacuum boundary ($q_\psi=2.1$).

In order to determine whether such a scenario is feasible, we analyze the axisymmetric stability of the race-track at four representative "snapshots" during its evolution (Fig. 1). We do not consider here the real-time transition from one equilibrium to the next. We assume that this happens slowly, so that all intermediate states can be considered as quasi-static equilibria. The resistive plasma evolution, as well as shape control problems and the effects of a non-ideal shell will be discussed elsewhere [6].

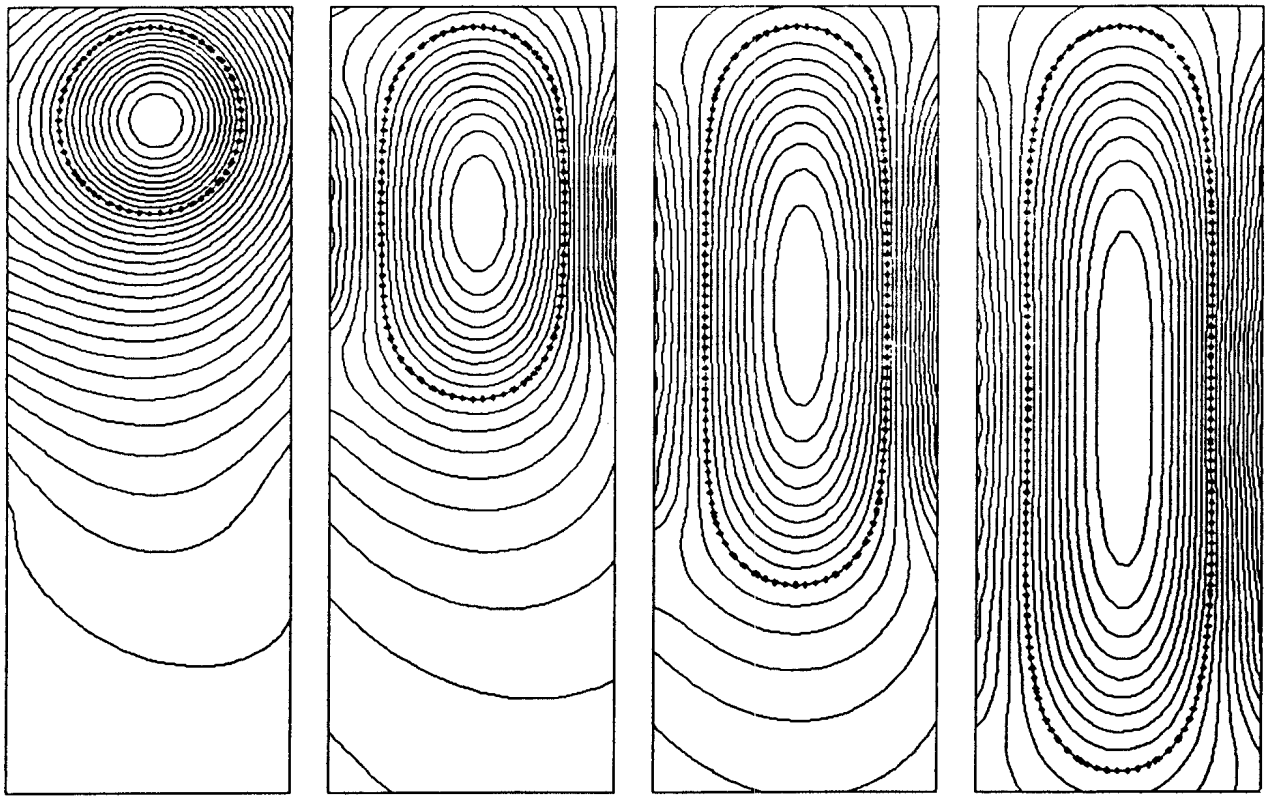

Fig.1.: Startup Scenario for Elongated Tokamak (k= b/a)

III. AXISYMMETRIC STABILITY. We compute the growth rate of the dominant vertical mode by using the FBTS code [7], which assumes an ideal MHD plasma within a perfectly conducting shell. The shell has no gaps so that both toroidal and poloidal image currents can flow freely. Plasma surface currents are excluded.

Figure 2 shows the growth rate as a function of the lateral plasma-wall distance for the four equilibria shown in Fig. 1. The parameter Δ is the distance between the plasma surface and the vertical walls (measured at the height of the magnetic axis) divided by the horizontal minor radius, a. The top-wall distance is assumed constant (Δ_{top}=0.22 at $R=R_o$). Note that the growth rates are normalized by the Alfvén frequency, $\omega_A^2 = B_o^2/(\mu_o \rho_o R_o^2)$, and that negative values of ω^2 indicate stable oscillations whereas positive values imply unstable growth. We observe that for $\Delta < 0.32$, all four equilibria are stable. Furthermore, we note that the marginal points for k=3 and k=4 almost coincide. This is caused by the cancellation of a destabilizing effect (vertical elongation) and a stabilizing effect (closeness of the bottom wall) as one goes from k=3 to k=4.

Vertical stability is extremely sensitive to variations in the width of the current profile, as shown in Fig. 3. Here, we plot the growth rate as a function of the profile parameter, ℓ. We also show the normalized width, w, defined as the FWHM of the radial current profile, divided by 2a. It is seen that a stable equilibrium which is quite far from the marginal point, such as the one with k=3, ℓ=-0.5 in Fig. 3., can be driven unstable by changing the normalized width by only 7%. It is clear that broad current profiles will be crucially important for a successful startup scenario.

IV. CONCLUSION. We have shown that startup scenarios for highly elongated tokamaks can be found such that all intermediate states are stable against axisymmetric, ideal MHD modes. These scenarios are characterized by broad current profiles (FWHM about 80% of the horizontal plasma diameter) and close lateral walls (plasma-wall distance less than 25% of the horizontal minor radius).

Acknowledgements This work was partly supported by the Swiss National Science Foundation.

References

[1] F. Troyon et al., Plasma Physics 26A (1983) 209.

[2] A. Sykes et al., in Europhysics Conference Abstracts (Proc. 11th European Conf. on Controlled Fusion and Plasma Physics, Aachen 1983) Vol. 7D, Part II, p. 363.

[3] R.D. Stambaugh et al., in Plasma Physics and Controlled Nuclear Fusion Research (Proc. 10th Int. Conf. London 1984) paper IAEA-CN-44/A-IV-2-1.

[4] M. Okabayashi et al., ibid., paper IAEA-CN-44/A-IV-3.

[5] F. Hofmann, Lausanne Report INT 110/82.

[6] F. Hofmann, F.B. Marcus, S.C. Jardin, to be published.

[7] F. Hofmann, F.B. Marcus, A.D. Turnbull, Lausanne, Report LRP 266/85.

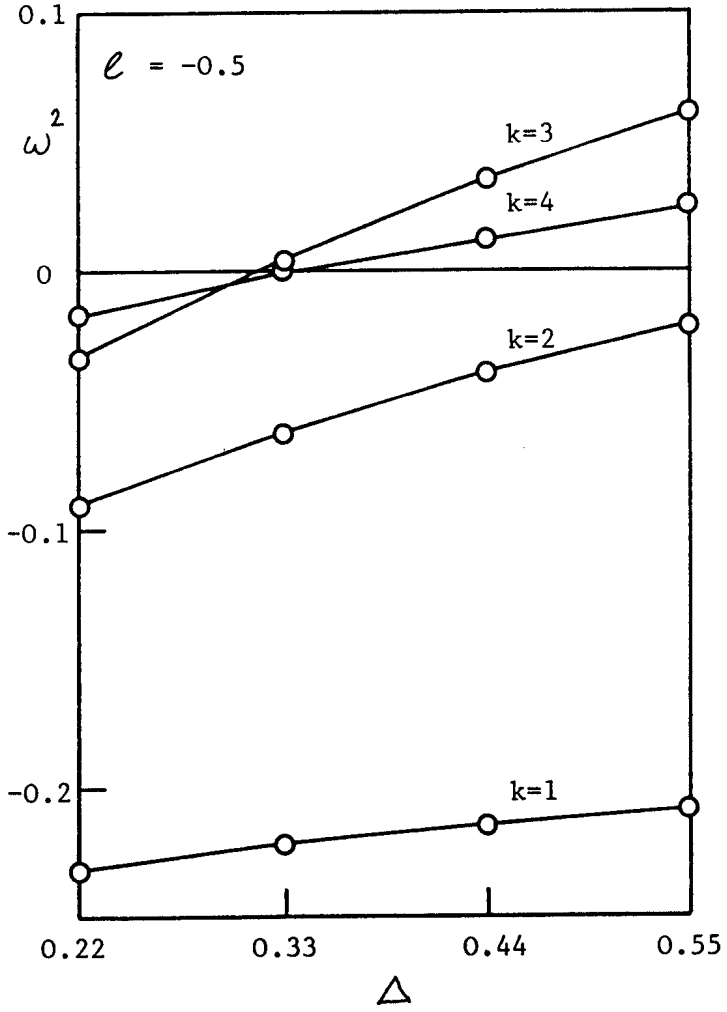

Fig.2. Normalized Growth Rate vs. Plasma-Wall Distance, Δ

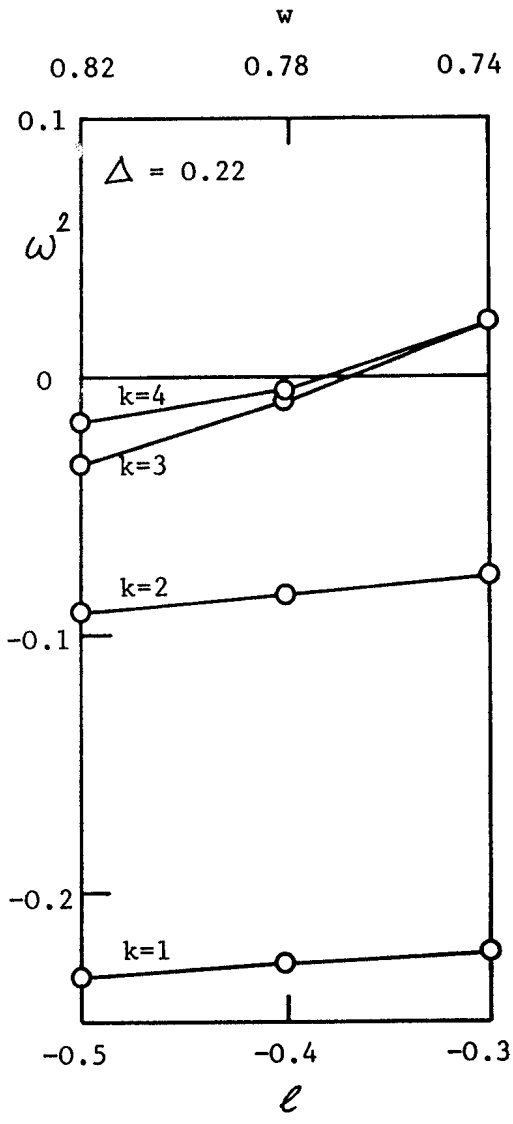

Fig.3. Normalized Growth Rate vs. Profile Parameter, ℓ